Atmos. Chem. Phys., 26, 2103–2116, 2026
https://doi.org/10.5194/acp-26-2103-2026

Atmospheric Chemistry and Physics
Open Access
EGU

Elucidation of the myrcene ozonolysis mechanism from a Criegee Chemistry perspective

Meifang Chen[1,2], Shengrui Tong[1], Shanshan Yu[1], Xiaofan Lv[1,2], Yanyong Xu[1,2], Hailiang Zhang[1], and Maofa Ge[1,2]

[1]State Key Laboratory for Structural Chemistry of Unstable and Stable Species, Beijing National Laboratory for Molecular Sciences (BNLMS), Institute of Chemistry Chinese Academy of Sciences, Beijing 100190, P.R. China
[2]University of Chinese Academy of Sciences, Beijing 100049, P.R. China

Correspondence: Shengrui Tong (tongsr@iccas.ac.cn)

Received: 3 September 2025 – Discussion started: 16 September 2025
Revised: 29 January 2026 – Accepted: 3 February 2026 – Published: 10 February 2026

Abstract. Criegee intermediates (CIs) are highly reactive species generated during the alkene ozonolysis, which play a critical role in atmospheric chemistry. Myrcene is a typical monoterpene, and its linear structure is significantly different from other cyclic monoterpenes such as α-pinene. This structural distinction consequently leads to different reactions mechanisms. This study employs a combined approach of matrix isolation Fourier transform infrared spectroscopy (MI-FTIR) and smog chamber experiments to elucidate the mechanisms of myrcene ozonolysis from the Criegee chemistry perspective. C3-CIs are captured at 880 cm^{-1} by using MI-FTIR. Ordered oligomers, which contain C3-CIs as chain units, are detected as significant components in secondary organic aerosol (SOA). These oligomers are formed via $RO_2 + n$ C3-CIs + HO_2/RO_2 mechanisms. C7-CIs are more prone to unimolecular decomposition to form C7-RO_2 radical, which act as initiators for oligomerization reactions. The mechanisms may also exist in other monoterpenes ozonolysis, which offering new insights into the contribution of CIs to SOA formation. Furthermore, the effect of the synergistic interaction between SCIs oligomerization and RO_2 autoxidation is illustrated. The mechanisms facilitate the rapid formation of highly oxygenated species, playing a critical role in particle nucleation. The increase in relative humidity can effectively reduce the formation of higher-order oligomers, thereby suppressing the SOA yield. This study provides a systematic elucidation of myrcene ozonolysis mechanisms, thereby significantly enhancing the understanding of oxidation processes in acyclic monoterpenes.

1 Introduction

Criegee Chemistry has long been recognized as playing an important role in the tropospheric atmosphere. Multiple model simulations have yielded atmospheric concentrations of stabilized Criegee intermediates (SCIs) of around 10^4–10^5 molecules cm^{-3} (Khan et al., 2018; Chhantyal-Pun et al., 2020). The concentration of OH radical is about 10^6 molec. cm^{-3} (Ringsdorf et al., 2023; Hofzumahaus et al., 2009; Lelieveld et al., 2016). Typically, if k_{SCI} is $\sim$100 times larger than k_{OH}, this is enough to make the rate of loss for reaction with SCIs comparable to that for reaction with OH radical. SCIs can undergo rapid reactions with many common trace molecules in the atmosphere, such as SO_2, organic acids, and amides, which are also faster than that reactions with OH radical (Long et al., 2025; Welz et al., 2014; Chhantyal-Pun et al., 2015; Mauldin et al., 2012). Recent study has shown that SCIs are significantly more efficient at removing greenhouse gases ($(CF_3)_2CFCN$) than OH radical (Jiang et al., 2025). The reaction with water vapor is the main removal pathway for SCIs due to the high abundance of water vapor in the atmosphere. The reaction rates of SCIs of different configurations with water vapor are found to be 10^{-11}–10^{-20} cm^3 molec.$^{-1}$ s^{-1}. Among them,

the reaction rate of syn-CH_3CHOO with H_2O is approximately 10^{-19}–10^{-20} cm^3 $molec.^{-1}$ s^{-1}, while the reaction rate of anti-CH_3CHOO with H_2O is faster, at approximately 10^{-14} cm^3 $molec.^{-1}$ s^{-1} (Vereecken et al., 2022; Yin and Takahashi, 2018; Lin et al., 2016; Anglada and Sole, 2016; Taatjes et al., 2013). The reaction has a pronounced conformational dependence, leading to large differences in reaction rates. Similarly, the reactivity of SCIs unimolecular decomposition is also conformation-dependent. Compared to anti-CIs, syn-CIs are more prone to undergo unimolecular decomposition reactions (Long et al., 2018, 2019; Vereecken et al., 2017).

The unimolecular decomposition process of SCIs, as well as bimolecular reactions involving organic acids, RO_2, etc. contribute significantly to the formation and growth of atmospheric secondary organic aerosol (SOA) (Boy et al., 2013; Chen et al., 2022; Zhao et al., 2015). Both field observations and laboratory studies have revealed that smaller-sized SCIs (species with carbon numbers $C \leq 4$) undergo sequential oligomerization reactions with RO_2 and organic acids, leading to the formation of low volatility organic compounds (LVOCs) or extremely low volatility organic compounds (ELVOCs) (Luo et al., 2025). Oligomers with CH_3CH_2CHOO (SCIs) as chain units were observed during the trans-3-hexene ozonolysis process (Zhao et al., 2015). Early studies on ethylene ozonolysis also identified oligomers formed from the reaction of multiple CH_2OO with organic acids (Sakamoto et al., 2013; Chen et al., 2021). Caravan et al. observed the oligomer sequence obtained through the continuous reaction of formic acid and six CH_2OO in the Central Amazon region (Caravan et al., 2024). These direct evidence indicates that SCIs contribute to SOA formation by oligomerization. These oligomerization mechanisms are now widely observed in the ozonolysis of alkenes that generate small-sized SCIs. Relative humidity (RH) may affect ozonolysis systems through the direct reactions between water vapor and SCIs. Zhang et al. (2023) found that SOA yield from limonene ozonolysis gradually increased with increasing RH, while SOA yield from Δ^3-carene ozonolysis decreased slightly. They attributed this phenomenon to the differing volatility of the products resulting from the reaction of structurally distinct CIs generated from the ozonolysis of these two monoterpenes with H_2O. Quantum chemical calculations have revealed that multiple SCIs may undergo oligomerization reactions with hydroperoxide esters (the products of the reaction of CH_2OO with water) to form oligomers with lower volatility (Chen et al., 2019). Increasing RH has been found to result in lower SOA yields and reduced oligomerization during the cis-3-hexenol ozonolysis (Harvey et al., 2016). The addition of water alters the reaction mechanism of SCIs in the ozonolysis system, leading to changes in the particle composition, which in turn affects the SOA yield. This indicates that RH is a key factor influencing the ozonolysis mechanism.

Monoterpenes ($C_{10}H_{16}$) are emitted into the atmosphere at a mean global rate of 95×10^6 metric tons of carbon per year, and contribute significantly to the global SOA budget. The yields of SCIs obtained from monoterpene ozonolysis range from approximately 0.2 to 0.60 (Sipilä et al., 2014; Zhang and Zhang, 2005; Gong and Chen, 2021; Cox et al., 2020; Newland et al., 2018). The production of SCIs leads to the occurrence of numerous SCIs-related reactions. Products derived from SCIs are also significant components of the SOA generated from monoterpene ozonolysis. Both in the α-pinene and limonene ozonolysis, specific mechanisms have been proposed in which both the unimolecular channels and the bimolecular reactions of SCIs contribute to the formation of SOA (Zhao et al., 2021; Zhang et al., 2023). The emissions of myrcene account for 2 % to 10 % of total biogenic monoterpene emissions (Sindelarova et al., 2014; Helmig et al., 2013). In addition to biogenic emissions, myrcene can also be present in indoor air (Kostiainen, 1995). The reaction with O_3 is one of the main removal pathways for myrcene, and plays an important role in the particle formation in the atmosphere. Myrcene is a straight-chain alkene containing both a conjugated π system, similar to that of isoprene (CH_2 =CH−C(=CH_2)-moiety), and a second part, structurally analogous to 2-methyl-2-butene $(CH_3)_2$C=CH-moiety, which is different from most of the widely studied cyclic monoterpenes (e.g., α-pinene, limonene). Such structural differences may give rise to variations in the reaction mechanisms and kinetics. The reaction rate of myrcene with O_3 is 3.8×10^{-16} cm^3 $molecule^{-1}$ s^{-1}, approximately 50 times faster than that of α-pinene ozonolysis and nearly 2 times faster than that of limonene ozonolysis (Deng et al., 2018; Atkinson et al., 1990; Cox et al., 2020; Munshi et al., 1989). About 99 % of the O_3 addition reactions with myrcene occur at the isolated double bond ($(CH_3)_2$C=CH−CH_2− moiety) (Deng et al., 2018). Therefore, the myrcene ozonolysis can lead to the formation of two CIs, $C_7H_{10}O_2$ (C7-CIs) and $C_3H_6O_2$ (C3-CIs). For cyclic monoterpenes such as α-pinene and limonene, their ozonolysis processes can only produce larger CIs containing ten carbon atoms (C10-CIs). Current studies have not confirmed that the C10-CIs generated from monoterpene ozonolysis can contribute to SOA formation through oligomerization. This suggests that the contribution mechanisms of CIs of different sizes produced during monoterpene ozonolysis to SOA formation may differ. Further studies are needed to elucidate the distinct roles of these CIs with different molecular sizes in SOA formation mechanisms, as well as the influence of their interactions on particle formation.

In this work, matrix isolation technology combined with vacuum Fourier transform infrared spectroscopy (MI-FTIR) and a smog chamber were employed to investigate the roles of both C3-CIs and C7-CIs in the myrcene ozonolysis. MI-FTIR was used to characterize the key intermediates produced in the early stage of myrcene ozonolysis, which to confirm the formation of stable C3-CIs and C7-CIs. To get

the contribution mechanism of C3-CIs and C7-CIs to SOA, we also performed the smog chamber experiments in various conditions during myrcene ozonolysis. RH was also considered as a significant factor influencing the ozonolysis mechanism and taken as an experimental variable. By analyzing the yields and molecular compositions of SOA, we elucidated distinct formation mechanisms through which varying molecular sizes of CIs contribute to SOA formation. Integrating these advanced techniques effectively improved the understanding of myrcene-derived SOA formation mechanism from the Criegee chemistry perspective.

2 Materials and methods

2.1 Matrix isolation experiment

Myrcene (97 %, Aladdin) was further purified through three freeze-pump-thaw cycles before being stored as a liquid in a storage tube. An O_2/O_3 mixture was generated by passing high-purity O_2 ($\geq$ 99.999 %) at a flow rate of 200 mL min^{-1} through an ozone generator (Beijing Tonglin Technology Co., Ltd.). The collected O_2/O_3 mixture was frozen in liquid nitrogen and undergoes several cycles of freeze-pump-thaw to remove the residual impurity gas. O_3 or myrcene, in a 1 : 100 ratio with Ar, was mixed and stored in a 5 L spherical glass container. The matrix was maintained at 6 ± 1 K within a closed-cycle helium refrigerator (Physike Technology Co., LTD, Qcryo-Scryo-S-300). The characteristic infrared peaks of initial ozonolysis products were detected by using a Fourier transform infrared spectrometer (Bruker Vertex 70v) equipped with a liquid nitrogen-cooled mercury-cadmium-telluride (MCT) detector. Measurements spanned 600–4000 cm^{-1}, employing 32-scan averaging and 0.5 cm^{-1} resolution. The experimental chamber was maintained under a vacuum of 10^{-5} Pa. The deposition of myrcene/Ar and O_3/Ar onto the 6 ± 1 K cold window was facilitated by two angled and independent tubes at a rate of 5 mL min^{-1}. This deposition was known as the twin-jet co-deposition mode. The deposition duration was approximately 120 min. To allow limit the diffusion and/or reaction of reactants, these matrices were heated or annealed to 35 K and held for 0.5 h, and then cooled to 6 ± 1 K after which the spectra were recorded. To promote the further occurrence of the reaction and further soften and diffuse the matrix, the matrix was further heated to 45 and 55 K (Yu et al., 2025; Yang et al., 2020). To prevent matrix loss, it was imperative to immediately cool down to 6 ± 1 K after reaching the target temperature and to record the spectra.

2.2 Particles generation and collection

The myrcene ozonolysis experiments were performed in a 1.2 m^3 atmospheric simulation Teflon chamber maintained at room temperature (24 ± 1 °C) under different RH conditions. Myrcene was introduced into the chamber by passing zero air through a heated three-way U-shaped tube. The n-hexane was conducted in a consistent manner. The addition of approximately 367 ppm of n-hexane resulted in the removal of approximately 98 % of OH radical. The O_2/O_3 mixture was generated in the same manner as described above. The O_2/O_3 mixture was introduced in a single injection via a syringe and was not replenished during the experiment. The O_3 concentration was monitored by an O_3 analyzer (Thermo Scientific model 49i) throughout myrcene ozonolysis. The measurement of the myrcene concentration was conducted by means of a gas chromatograph with a quadrupole mass spectrometer (GC-MS, Agilent, 7890, 5977B) equipped thermal desorption instrument (TD). The GC-MS is on an HP-5MS column (30 m $\times$ 0.25 mm $\times$ 5 µm) with helium as carrier gas and a flow rate of 1.2 mL min^{-1}. The temperature of the chromatographic column was set as follows: the initial temperature was 40 °C and held for 3 min. The temperature was then increased to 140 °C by maintaining a rate of 20 °C min^{-1}; the program was then finished by increasing the temperature to 200 °C at a rate of 25 °C min^{-1}. Organics were quantified in selected ion monitoring (SIM) mode and 41 m/z, 69 m/z and 93 m/z were selected as the characteristic ions detected by mass spectrometry for myrcene. The maintenance of different RH levels was achieved by the implementation of a 10 L min^{-1} flow of zero air through the water bubbler. The indoor temperature and RH were measured using a hygrometer (Vaisala, HMP3). Throughout each experiment, size distributions and volume concentrations of particles were continuously recorded using a scanning mobility particle sizer (SMPS), which consisted of a differential mobility analyzer (DMA, TSI, Model 3081) and a condensation particle counter (CPC, TSI, Model 3776). The SMPS measured particles every 3 min across a size range of 14.3 to 723.4 nm. A sampling flow of 0.3 L min^{-1} and a sheath flow of 3.0 L min^{-1} were used. The yield of SOA was obtained by the ratio of the maximum mass concentration of the corrected particles to the mass concentration of myrcene consumed (Liu et al., 2024; Chen et al., 2022). The specific equation was as follows.

$$Y_{SOA} = \frac{M_{SOA}}{\Delta M_{VOC}} \quad (1)$$

Here, Y_{SOA} represented the SOA yield, M_{SOA} denoted the maximum mass concentration of particle after wall-loss correction during the reaction process, and ΔM_{VOC} referred to the total consumption mass concentration of VOCs throughout the reaction.

The average effective density of SOA obtained from the myrcene ozonolysis is 1.25 g cm^{-3} (Boge et al., 2013). The SOA was sampled after 3 h of reaction, with a sampling duration of approximately 60 min. The SOA particles generated within the chamber were captured on a 25 mm PTFE filter (Sartorius, 0.45 µm pore size) and subsequently analyzed using an ultra-high performance liquid chromatography with a Quadrupole-Orbitrap mass spectrometer equipped with

an electrospray ionization source (UHPLC/ESI-MS, UPLC, UltiMate 3000, Thermo Scientific, ESI-MS, Q-Exactive, Thermo Scientific) equipped with a Hypersil GOLD C18 column (2.1×100 mm, 1.9 µm packing size). The collected particle sample was eluted with 0.5 mL of methanol (Optima™ LC/MS Grade, Fisher Chemical) into a sample bottle. Mass spectrometric analysis utilized positive ion mode, scanning a molecular weight range of m/z 50–750 Da. The elution flow rate was set at 0.2 mL min^{-1} with a total run time of 4.0 min. An injection volume of 10 µL was used. In positive ion mode, three ionic forms of particulate components were identified, specifically $[M+H]^+$, $[M+Na]^+$ and $[M+NH_4]^+$. Tandem mass spectrometry (MS/MS) was employed to elucidate component structures within the SOA. The isolation width of 1.2 m/z units was applied. The electrospray ionization source was operated at a spray voltage of 3.0 kV and a capillary temperature of 300 °C, with sheath and auxiliary gas flows set to 35 and 10 Arb units, respectively. Both scans were performed at a resolution setting defined at m/z 200, with values of $R = 70\,000$ for the MS scan and $R = 17\,500$ for the MS/MS scan. Data acquisition and processing were conducted using Xcalibur software (version 3.0).

2.3 Quantum chemistry calculations

Additional quantum chemical calculations were performed to compare with the experimentally obtained infrared spectra. The geometries of the myrcene, primary ozonides (POZs) and SCIs were optimized using the hybrid density functional theory B3LYP-D3(BJ) with the aug-cc-pVTZ basis set. Harmonic vibrational frequencies were calculated at the B3LYP/6-311G++(d,2p) calculation level for the comparison with the experimental infrared peak. Various computational levels for CIs were compared, and the one with superior performance was selected accordingly. Please refer to Table S1 in the Supplement for the specific comparison. This method has been proved to be applicable to the relevant calculations of the SCIs system (Chen et al., 2025; Lin et al., 2018; Yu et al., 2025). The above-mentioned related calculations were all performed by using Gaussian 16 software package (Frisch et al., 2016). Molclus 1.1.2 in conjunction with the xtb software package was used to perform a systematic conformational search for myrcene, POZs and SCIs (Lu, 2023). The single-point energy was further calculated at the DLPNO-CCSD(T)/CBS level by using ORCA 5.0 software to obtain the Boltzmann distribution of each conformation more accurately (Neese, 2022).

3 Results and Discussion

3.1 Criegee chemistry in myrcene ozonolysis

$C_7H_{10}O_2$ (C7-CIs) and $C_3H_6O_2$ (C3-CIs) were produced from myrcene ozonolysis. The initial ozonolysis mechanism of myrcene has been established as shown in Fig. 1 based on the current studies. The products generated along with C7-CIs and C3-CIs were acetone and 4-vinyl-4-pentental (C7-aldehyde) with yields of 0.27 and 0.73, respectively (Deng et al., 2018). The nascent C7-CIs and C3-CIs, possessing high internal energy, rapidly degraded in part. This process could contribute to the formation of OH radical (Reactions R2 and R3). The unimolecular isomerization pathways of CIs were strongly configuration-dependent. Syn-C7-CIs were mainly isomerized by 1,4-H transfer to form vinyl hydroperoxide (VHP), which decomposed to form OH radical and a vinoxy or β-oxo alkyl radical (Reactions R2 and R4). Anti-C7-CIs mainly proceed via an initial rearrangement (1,3 ring-closure) to form a dioxirane intermediate. Then the dioxirane intermediates could isomerize to form organic acid (Reactions R3 and R5). $C_3H_6O_2$ isomerized mainly through the formation of VHP. Another portion was collisional stabilized, forming SCIs (Reaction R1) (Criegee, 1975; Hassan et al., 2021; Jr-Min Lin and Chao, 2017; Khan et al., 2018). A portion of the SCIs might undergo unimolecular decomposition reactions, while another portion primarily engaged in bimolecular reactions with trace gases in the atmosphere (Jr-Min Lin and Chao, 2017; Kidwell et al., 2016; Su et al., 2014; Vereecken et al., 2012). The yields of OH radical and SCIs obtained from the myrcene ozonolysis were 0.63 ± 0.09 and 0.30, respectively (Aschmann et al., 2002; Cox et al., 2020; Newland et al., 2018).

Although previous studies had provided some references to the initial ozonolysis mechanism of myrcene, the presence of CIs had only been demonstrated deductively. In this study, MI-FTIR was employed to capture the key intermediates formed during the initial ozonolysis of myrcene. As shown in Fig. 2, some new bands were observed in the spectra obtained by the twin-jet co-deposition. Most of the absorption peaks of the products grew with rising temperature within the 35–55 K interval. This observation indicated that the myrcene initial ozonolysis occurred when the Ar matrix softened and diffused. The new bands were located at 765, 880, 905, 1074, 1177, 1370 and 1720 cm^{-1}. The spectra of a single precursor (Myrcene/Ar or O_3/Ar) obtained after annealing at different temperatures as comparison was shown in Fig. S1 in the Supplement.

The characteristic IR vibrational bands of the POZs, formed via initial cycloaddition between myrcene and O_3, were localized on its 1,2,3-trioxolane ring. These included asymmetric O-O-O stretching and C-O stretching vibrations within the five-membered ring structure (Wang et al., 2020). The presence of two different configurations in POZs was attributable to the varying orientations of the central O atom on the five-membered ring. The peaks calculated from the asymmetric stretching vibration in both POZs configurations overlapped at 772 cm^{-1}. Moreover, O-O-O asymmetric stretching vibrations of POZs were commonly observed within the 700–800 cm^{-1} spectral region as documented in prior literature (Yang et al., 2020; Wang et al., 2020). Thus, the band at

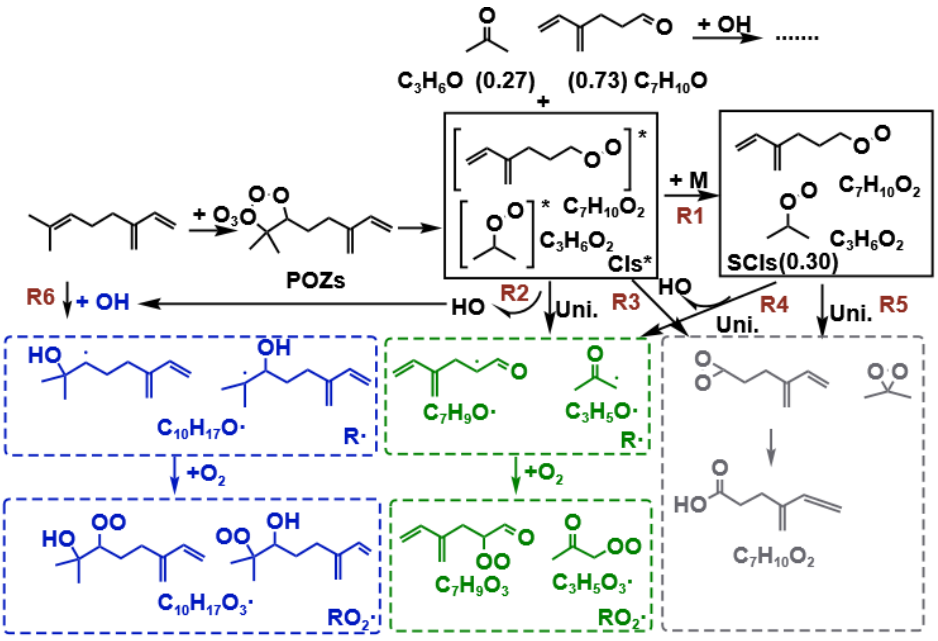

Figure 1. Proposed the key pathway in the initial ozonolysis of myrcene. The values in parentheses represent the yields of the corresponding products. The blue boxes indicate OH-derived products. Green-shaded boxes represent products formed via unimolecular reaction of *syn*-CIs through the vinylhydroperoxide (VHP) channel followed by O_2 addition. Gray-shaded boxes correspond to products generated from unimolecular reaction of *anti*-CIs via 1,3-ring-closure.

765 cm^{-1} which obtained from the twin-jet experiment was assigned to the O-O-O asymmetric stretching vibration of POZs. The calculation results indicated that the C-O stretching vibrations of the two POZs were located at positions 1059 and 1165 cm^{-1}. The newly emerged peaks at positions 1074 and 1177 cm^{-1} corresponded to the C-O stretching vibration of POZs in the twin-jet spectra. Moreover, these POZ-related infrared peaks emerged at 35 K, and their intensity increased with rising annealing temperature until distinct infrared peaks became apparent at 55 K.

The main conformers and the infrared vibration frequencies of C3- and C7-CIs were obtained through quantum chemical calculations. The strongest characteristic infrared vibration peak of CIs was caused by O-O stretching vibration (Su et al., 2013; Lin et al., 2015). The extant research results indicated that the characteristic infrared peak caused by the O-O stretching vibration of C3-CIs in the gas phase located at 887 cm^{-1} (Wang et al., 2016). In the twin-jet spectra, a distinct new peak was observed at position 880 cm^{-1} at 55 K, which was likely to be attributed to the C3-CIs. The resulting $\sim$ 7 cm^{-1} deviation might be attributable to the Ar matrix effect (Bach, 1999). The calculated O-O stretching vibrations of C7-CIs were located at 882 (syn-C7-CIs) and 910 (anti-C7-CIs) cm^{-1}. According to Table S1 in the Supplement, the calculated IR peaks of CIs were consistently overestimated by over 10 cm^{-1} relative to experimental values, with the deviation being most pronounced for anti-CIs. Notably, no distinct new peaks appeared below 882 cm^{-1} in the experiment. This absence suggested that very few stabilized C7-CIs were likely generated during the ozonolysis of myrcene. Instead, most C7-CIs were consumed via unimolecular decay pathways, this conclusion which was also supported by our subsequent analysis.

In addition to the early intermediates, acetone was identified as a major product co-produced with C7-CIs in myrcene ozonolysis. The spectral bands of 1370 and 1720 cm^{-1} appeared in the twin-jet spectra belong to acetone (Han and Kim, 1996). The generation of acetone also indirectly demonstrated the formation of C7-CIs. The peak at 905 cm^{-1} coincided in temperature with the C3-CIs peaks and suggested its assignment to the $=CH_2$ wagging vibration of the C7-aldehyde. MI-FTIR experiments unequivocally verified that myrcene ozonolysis proceeded via the Criegee mechanism. Furthermore, both C3- and C7-CIs were generated during this process.

3.2 Impact of CIs on SOA generation

To explore the contribution of CIs to the SOA generation, the myrcene ozonolysis experiments were conducted under different conditions (with or without an OH scavenger and at varying RH levels) in a 1.2 m^3 smog chamber (Table 2). The unimolecular decay of both excited CIs and SCIs could produce OH radical. Therefore, SOA formation included contributions from both SCIs and OH radical derived in myrcene ozonolysis.

Table 1. Identification and assignments of experimental absorption bands in the initial ozonolysis of myrcene.

Experimental bands/(cm^{-1})	Calculated Band/(cm^{-1})	Reference	Belonger	Assignment[c]
765	772	–	POZs	O-O-O str.
880	–	887[a]	C3-CIs	O-O str.
905	–	–	4-vinyl-4-pentena	$=CH_2$ wag.
1074	1054	–	POZs	C-O str.
1177	1165	–	POZs	C-O str.
1370	–	1370[b]	Acetone	δ CH_3
1720	–	1721.6[b]	Acetone	C=O str.

Note: [a] The characteristic infrared peaks of gas-phase C3-CIs measured by step-scanning Fourier transform infrared spectroscopy (Wang et al., 2016). [b] Measure in the low- temperature Ar matrices (Han and Kim, 1996). [c] str. stands for stretching vibration; wag. stands for wagging vibration; δ stands for the scissoring vibration.

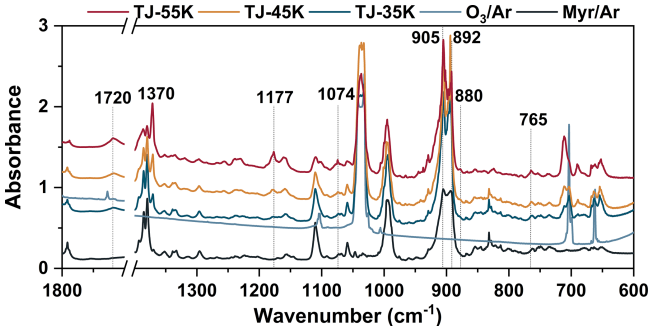

Figure 2. The twin-jet IR spectra of myrcene ozonolysis reaction in a low temperature and Ar matrix after annealing to 35, 45 and 55 K. The blank spectra of myrcene/Ar and O_3/Ar were also given. T-J means the spectra obtained by twin-jet method.

As shown in Table 2, Exp. 1–2 added n-hexane (HA) as an OH radical scavenger to highlight the contribution of SCIs-derived pathways. Exp. 3–5 were conducted with progressively increasing RH to modulate SOA formation by introducing direct reactions between water and SCIs. The volume concentration of the particles rose sharply within approximately 30 min and reached its maximum value within 180 min (Fig. S2). The dominant size range of SOA expanded from 50–250 nm during myrcene ozonolysis (Fig. 3). The suppression of particle formation induced by the OH scavenger and elevated RH was conspicuously demonstrated. Following the 367 ppm HA addition, the particle yield from myrcene ozonolysis decreased by approximately 72 %. As RH increased from dry conditions to ∼20 % and subsequently to 50 %, the particle yield gradually declined by 17 % to 40 % (Table 2). As shown in Fig. 3a, after the addition of HA, no significant reduction in the particle size distribution was observed within the first 30 min. This might be attributed to the rapid reactions of SCIs, indicating that gas-phase reactions of SCIs played an important role in particle nucleation. Between 90 and 180 min of reaction, the particle size distribution decreased markedly. This reduction was due to the scavenging of OH radicals, which inhibited the formation of OH-RO_2 pathway. Bimolecular reactions and the autoxidation of OH-RO_2 played a crucial role in the growth of SOA (Baker et al., 2024). As the RH gradually increased from ∼20 % to 50 %, the growth of particle size was inhibited across different time periods. This phenomenon occurred because reactions between water and SCIs might prevent these compounds from converting into larger, less volatile products. Therefore, OH radical generated from CIs and SCIs also contributed to the growth of particle size distribution and enhanced SOA yield.

The O_3 concentration listed in the table is the value recorded after the O_3 analyzer stabilized for 20 min, which corresponds to the 20 min mark after the initiation of the experiment.

3.3 Mechanism of SCIs contribution to SOA

UHPLC-ESI-MS was employed to analyze the chemical compositions of SOA collected offline. CIs were important SOA precursors during the ozonolysis process. In this study, the contribution mechanisms of CIs to SOA formation were proposed in myrcene ozonolysis.

$C_{10}H_{18}O_5$ and $C_{10}H_{18}O_4$, with relative abundances (RA) of 76 % and 73 % respectively, ranked among the top 3 in the absence of any scavengers at RH < 0.5 % as shown in Fig. 4a. The formation of these two intense peaksbelonged to the contribution of OH radical oxidation processes. The OH radical was almost entirely originated from the CIs unimolecular decomposition reactions. The OH radical and O_2 reacted sequentially with myrcene to form $C_{10}H_{17}O_3$ radical (as shown in Fig. 1, Reaction R6). $C_{10}H_{17}O_3$ radical then underwent autoxidation channel which was highly likely to occur to produce $C_{10}H_{17}O_5$ radical (Jokinen et al., 2014). The reaction of $C_{10}H_{17}O_5$ radical with HO_2 yielded $C_{10}H_{18}O_5$ which was detected as the main product. Meanwhile, $C_{10}H_{17}O_5$ radical could also react with any RO_2 radical to yield $C_{10}H_{18}O_4$. The relative peak intensity of $C_7H_{10}O_2$ was slightly lower than that of $C_{10}H_{18}O_5$ and $C_{10}H_{18}O_4$, and its molecular formula

Table 2. Summary of experimental conditions.

Exp.	[Myrcene]/ppb	[O_3]/ppb	RH/ %	Scavenger	M_{SOA} (μg cm^{-3})	Y_{SOA}
1	171.5	~200	< 0.5	–	346	0.36
2	170	~200	< 0.5	~367 ppm HA	91	0.10
3	222	~200	< 0.5	–	509	0.41
4	231	~200	~20	–	432	0.34
5	230	~200	~50	–	311	0.24

Note: n-hexane is abbreviated as HA.

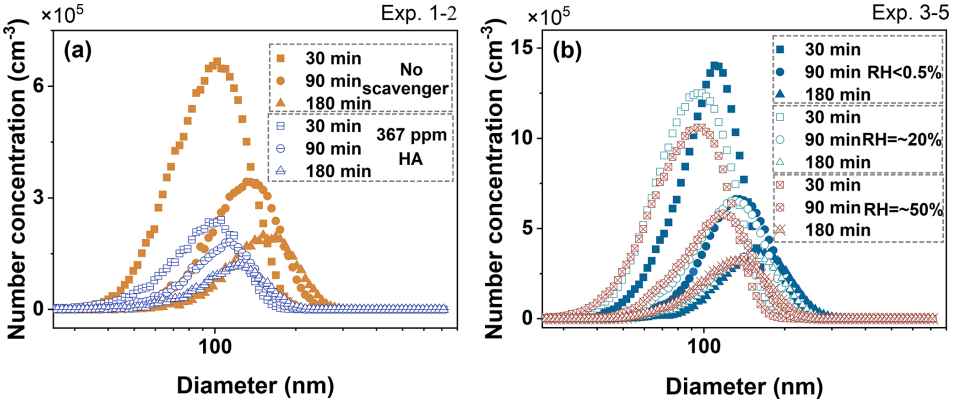

Figure 3. Time series of size distributions of aerosol particles formed at 30, 90, and 180 min after the initiation of myrcene ozonolysis under different conditions. **(a)** depicted particle formation processes corresponding Exp. 1–2 from Table 2, while **(b)** illustrated particle formation processes in Exp. 3–5 from Table 2.

was consistent with C7-CIs. It was inferred that it might originate from C7-OH produced during the unimolecular decomposition of C7-CIs. C7-CIs underwent unimolecular decomposition via the VHP pathway, producing OH radical while simultaneously generating R radical. The R radical subsequently reacted with O_2 to form $C_7H_9O_3$. $C_7H_9O_3$ could react with any RO_2 radical to form $C_7H_{10}O_2$ (C7-OH). The OH radical yield from myrcene ozonolysis was generally high, which also confirmed that the larger CIs generated during this process tend to react via unimolecular decay pathways (Cox et al., 2020).

$C_{10}H_{17}O_5$ radical, as the main RO_2 radical, could undergo sequential oligomerization. Several peaks representing ordered oligomers with $C_3H_6O_2$ as chain units were found. The chemical formula of $C_3H_6O_2$ was identical to C3-CIs and confirmed to existent by the matrix isolation experiment. The proposed pathway was shown in Reaction (R7). The rate constants for the reaction of RO_2 radicals with SCIs were much higher than that for ROOH (Zhao et al., 2017; Chao et al., 2024; Chhantyal-Pun et al., 2020; Caravan et al., 2024). $C_{10}H_{17}O_5$ radical reacted with one or two C3-CIs, followed by reaction with HO_2 radical resulting in chain termination ($C_{10}H_{17}O_5 + n$ C3-CIs + HO_2, $n = 0$–2, Sequence 1). However, the relative intensities of this set of oligomer signals were relatively low. This was likely because $C_{10}H_{17}O_5$ radical more readily reacted with HO_2 or RO_2 to form $C_{10}H_{18}O_5$ and $C_{10}H_{18}O_4$, thereby reducing the likelihood of its reaction with C3-CIs in the gas phase. These oligomer sequences exhibited similar distribution patterns of major fragment ion peaks in MS/MS spectra in Fig. S3a. Therefore, these oligomers with C3-CIs as the chain units had similar structural units in their chemical composition. Moreover, the corresponding structural assignments for its major fragment peaks were provided in Fig. S3b. The fragments $C_5H_7^+$ (m/z 67.06), $C_6H_9O_2^+$ (m/z 113.06), and $C_9H_{13}O^+$ (m/z 137.10) revealed that the oligomers in Sequence 1 all feature a carbon chain skeleton characterized by conjugated double bonds. The $C_3H_7O^+$ (m/z 59.05)/$C_3H_7O_2^+$ (m/z 75.05) fragment ions originated from cleavage of terminal -OH or -OOH functionalized tertiary carbon moieties in the oligomers. For C7-CIs, no significant oligomers with C7-CIs as chain units were observed when reacting with $C_{10}H_{17}O_5$ radical. Although the mass spectral peak corresponding to $C_{17}H_{28}O_7$ was observed and its molecular formula aligned with the expected product of $C_{10}H_{17}O_5$+ C7-CIs. But $C_{17}H_{28}O_7$ could also originate from $C_{10}H_{17}O_5$+ $C_7H_{11}O_4$ (the formation pathway as shown in Scheme S1). Moreover, $C_{17}H_{28}O_7$ was classified as a low-volatility organic compound (LVOCs) (Donahue et al., 2012; Donahue et al., 2011), which readily partitioned into the particle phase. But its low abundance implied $C_{17}H_{28}O_7$ did not appear as a dominant product. Consequently, the contribution

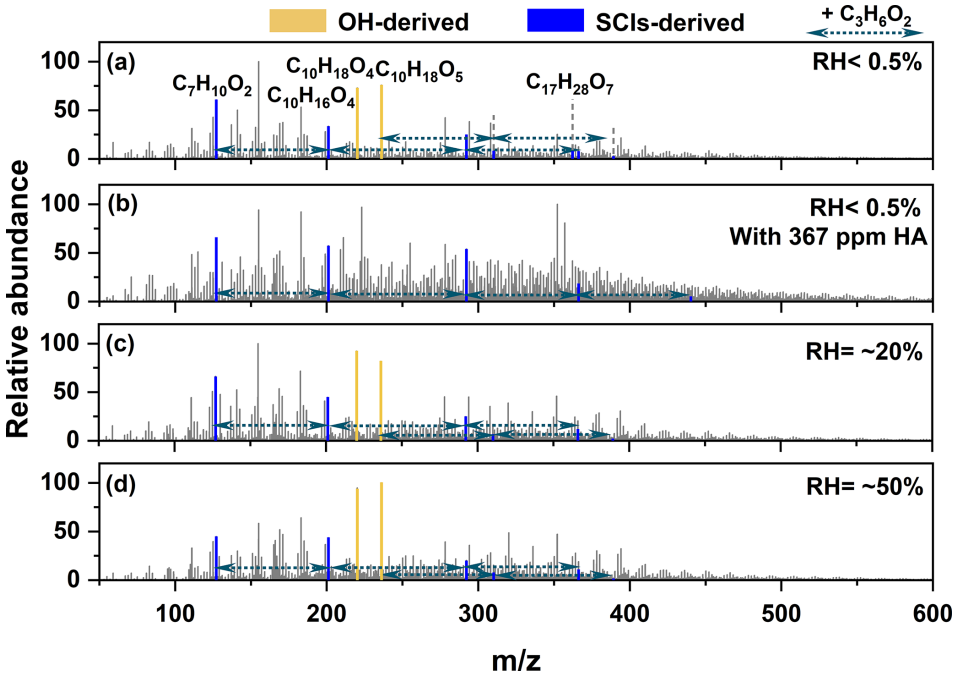

Figure 4. UHPLC/ESI-MS of SOA from myrcene ozonolysis in different conditions. **(a)** No scavenger was added. **(b)** 367 ppm n-hexane (HA) was added. **(c)** RH = ∼ 20 % condition. **(d)** RH = ∼ 50 % condition. The substances marked by the yellow lines originated from the OH-derived channel, while those marked by the blue lines mainly originated from the SCIs-derives channel. The oligomer sequence containing C3-CIs as the chain unit was marked by the green dotted line.

of C7-CIs oligomerization to myrcene-derived SOA formation might be considered negligible. In addition, an ordered oligomer sequence formed by $C_7H_{10}O_2 + n$ C3-CIs was also identified. The corresponding compounds in the sequence are $C_7H_{10}O_2$ (m/z 127.075), $C_{10}H_{16}O_4$ (m/z 201.112), $C_{13}H_{22}O_6$ (m/z 292.175) and $C_{16}H_{28}O_8$ (m/z 371.168), namely Sequence 2 (The peaks with relative abundance of less than 1 % were ignored). The proposed pathway of Sequence 2 was as shown in the Reaction (R8). Sequence 2 had a greater degree of oligomerization and contributed more to particle formation than Sequence 1. This indicated that $C_7H_9O_3$, which produced by C7-CIs unimolecular reaction, more readily reacted with C3-CIs in the gas phase. The oligomerization reactions within the Sequence 2 all terminated with the reaction of RO_2 radical ($C_7H_9O_3 + n$ C3-CIs + RO_2). Figure S4 presented the MS/MS spectrum of Sequence 2 along with the proposed structures corresponding to the major fragment peaks. The presence of fragments such as $C_5H_7^+$ (m/z 67.06), $C_7H_7O^+$ (m/z 95.05), and $C_6H_9O_2^+$ (m/z 113.06) indicated that the oligomers in Sequence 2 possessed a conjugated double-bond skeleton. This suggested that this sequence was initiated by C7 compounds. The fragment at m/z 71.05 ($C_4H_7O^+$) was generated via α-cleavage adjacent to a carbonyl group in the oligomer backbone. This fragmentation was typical of compounds containing conjugated carbonyl motifs and further supported the presence of a C7-based conjugated skeleton in the sequence. The $C_3H_7O^+$ (m/z 59.05) fragment ions originated from cleavage of terminal -OH functionalized tertiary carbon moieties in the oligomers. The formation of this ion fragment was similar to that in Sequence 1. In the MS/MS spectra of $C_{10}H_{16}O_4$, we observed that besides the fragment peaks annotated in Fig. S4, there existed fragment ion peaks with higher intensities. This suggested that $C_{10}H_{16}O_4$ was formed through multiple pathways (such as the RO_2+ RO_2 reaction) (Peräkylä et al., 2023; Frandsen et al., 2025). Consistently, no discernible oligomerization signals were detected for reactions using $C_7H_9O_3$ as the starting reactant with C7-CIs.

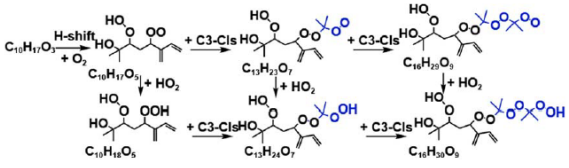

(R7)

As shown in Fig. 4b, the peaks corresponding to $C_{10}H_{18}O_4$ and $C_{10}H_{18}O_5$ disappeared after the addition of the OH radical scavenger, as expected. The $C_7H_{10}O_2$ peak remained, which further demonstrating that $C_7H_{10}O_2$ originated from SCIs-derived products. Compared to the mass spectrum without the scavenger, the contribution of the oligomers in Sequence 2 markedly increased. Following the introduction of the scavenger, the peak intensities corresponding to compounds with higher degrees of oligomerization ($C_{13}H_{22}O_6$ and $C_{16}H_{28}O_8$) within the sequence were significantly en-

hanced. Moreover, compared to the spectrum acquired in the absence of the scavenger, a more highly oligomerized compound ($C_{19}H_{34}O_{10}$) was detected. Water served as the dominant removal pathway for SCIs in the atmosphere. Correspondingly, the contribution of Sequence 2 to SOA formation decreased progressively with increasing RH as shown in Fig. 4c and d, especially substances with a higher degree of oligomerization in the sequence ($C_{13}H_{22}O_6$ and $C_{16}H_{28}O_8$). So, the Sequence 2 was primarily contributed by SCIs-derived.

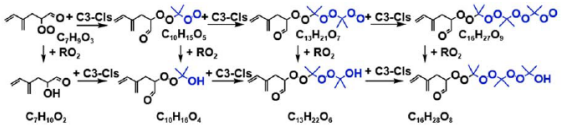

(R8)

Meanwhile, some compounds were found to have the same number of C and H atoms, differing only in the number of O atoms in parallel oligomer sequences, namely, $C_7H_{10}O_{2-5}$, $C_{10}H_{16}O_{4-7}$, $C_{13}H_{22}O_{6-9}$ and $C_{16}H_{28}O_{8-11}$ (Sequence 2N) as shown in Fig. 5a. Compounds with identical carbon and hydrogen atom counts exhibited closely resembling major fragment ions in their MS/MS spectra as shown in Fig. 5b. This suggested that compounds with identical carbon and hydrogen atom counts exhibited highly consistent formation pathways. The process leading to progressive oxygenation (i.e., increasing oxygen atom content) was the RO_2 autoxidation mechanism (Jokinen et al., 2014; Liu et al., 2023). Simultaneously, Sequence 2N was the oligomer series formed by oligomerization with C3-CIs as chain units. This indicated that SCIs oligomerization and RO_2 autoxidation mechanistically interplayed in the formation of Sequence 2N. The proposed formation mechanism of Sequence 2N was illustrated in Fig. 5c. RO_2 underwent oligomerization with n SCIs to form the oligomer RO_2-n SCIs, while concurrently undergoing autoxidation to generate R'O_2. R'O_2 might subsequently underwent analogous cycles of SCIs oligomerization and autoxidation. This radical propagation cascade ultimately terminated via reactions with RO_2 or HO_2 radical. SCIs inherently contained at least two oxygen atoms in their structure due to the presence of terminal -COO groups. The RO_2 autoxidation inherently involved reaction with O_2, which rapidly elevated the oxygen content in products. Consequently, the synergistic interplay between SCIs oligomerization and RO_2 autoxidation facilitated rapid formation of high-molecular-weight species and highly oxygenated molecules (HOMs), which substantially contributed to particle nucleation and growth.

The addition of different scavengers also affected the formation of Sequences 2N. Figure 6 illustrated the proportions of compounds with various oligomerization degrees of oligomerization in Sequence 2N under different scavenger conditions. The dominant compounds in Sequences 2N were $C_{13}H_{22}O_{6-9}$ which contained two C3-CIs as chain units under dry conditions, with or without added OH radical (Fig. 6a and b). Furthermore, following the addition of OH radical, the proportions of both $C_{13}H_{22}O_{6-9}$ and $C_{16}H_{28}O_{8-11}$ in Sequences 2N gradually increased (Fig. 6b). This indicated that the SCIs oligomerization reaction significantly contributed to the particle formation after the addition of the OH scavenger. This was consistent with the result observed in Sequences 2. As the RH increased, the main compound in Sequences 2N became $C_{10}H_{16}O_{4-7}$, which contained only a single C3-CIs as a chain unit (Fig. 6c and d). The proportions of both $C_{13}H_{22}O_{6-9}$ and $C_{16}H_{28}O_{8-11}$ in Sequence 2N decreased with increasing RH. This indicated that the reaction of water with C3-CIs directly affected the generation of oligomers with higher degrees of oligomerization. Additionally, the fraction of $C_7H_{10}O_{2-5}$ decreased significantly with increasing RH. This indicated that besides reacting with C3-CIs, water also scavenged C7-CIs to some extent. Therefore, the contribution of the SCIs oligomerization mechanism to SOA formation were suppressed under elevated RH conditions.

Sequence 1, 2 and 2N demonstrated ordered oligomers formed with C3-CIs as chain units. However, ordered oligomeric sequences ($RO_2 + n$ C7-CIs + HO_2/RO_2, $n \geq 2$) with C7-CIs as the chain unit were not discovered. Based on the current formation mechanism of oligomers, C3-CIs and C7-CIs differed in their contribution to particle formation in myrcene ozonolysis. For smaller molecular-sized CIs (C3-CIs), the primary pathway for partitioning into the particle involved oligomerization with RO_2 radical and other species. The C7-CIs had higher molecular masses than C3-CIs. The products from unimolecular and bimolecular reaction of C7-CIs partitioned more readily to particles which reduced the viability to function as chain units in oligomerization processes (Donahue et al., 2012; Donahue et al., 2011). Furthermore, C7-RO_2 generated from unimolecular decomposition of C7-CIs acts as a chain-initiating precursor that reacts with C3-CIs, thereby contributing to particle nucleation. These findings implied divergent dominant pathways for SOA formation mediated by SCIs across varying molecular dimensions in VOCs ozonolysis. The C10-CIs with high molecular weights generated during the ozonolysis of α-pinene and limonene might also be more likely to incorporate into the particle via unimolecular reaction mechanisms rather than through oligomerization. Our findings further demonstrated that when evaluating SCIs contribution pathways to SOA, the molecular size of SCIs might be prioritized especially during monoterpenes ozonolysis. The molecular size of SCIs might lead to differences in their primary mechanisms of contributing to SOA formation. In the myrcene ozonolysis system, the branching ratio might favor the formation of C3-CIs over C7-CIs, which further enhanced the propensity of C3-CIs toward oligomerization. Currently, no literature has elucidated the contribution mechanisms of CIs of different sizes to SOA formation from the perspective of molecular size. This study presented this concept for the first time.

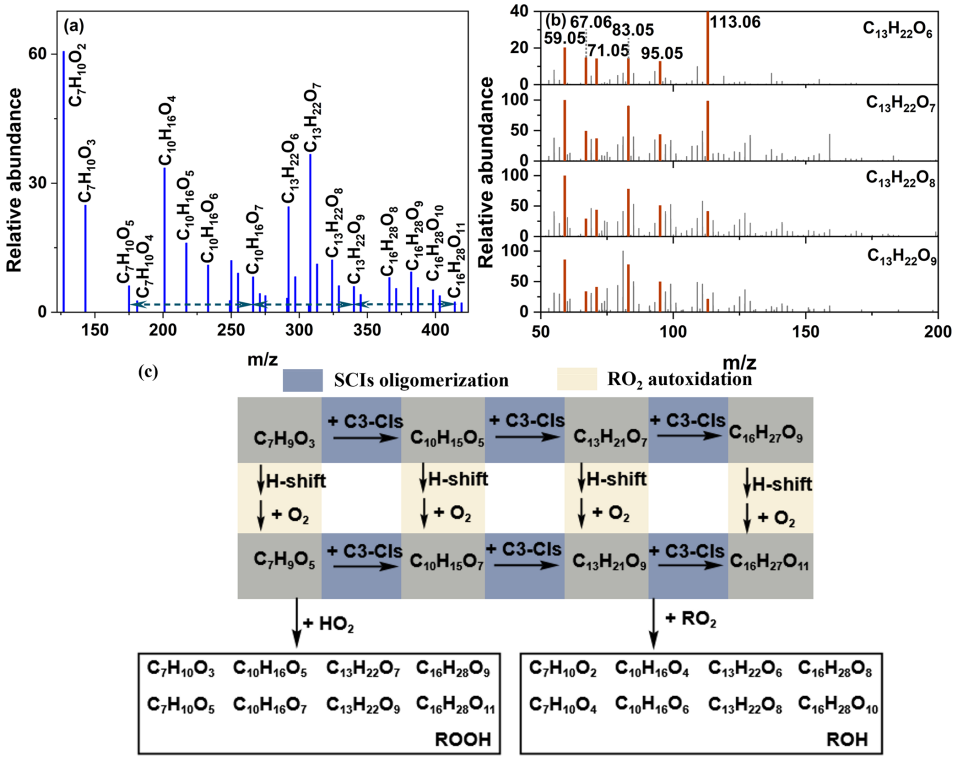

Figure 5. The relative abundance and the proposed pathways of oligomer sequences derived from the synergistic SCIs oligomerization and RO_2 autoxidation. **(a)** Mass spectrometric distribution of oligomeric sequences under dry conditions. **(b)** The MS/MS spectra of $C_{13}H_{22}O_{6-9}$ and the major fragment ions were highlighted in orange in the mass spectra. **(c)** The proposed mechanism of this oligomer sequences. The blue area denoted the SCIs oligomerization pathway. The yellow area represented the RO_2 autoxidation pathway. The black solid box indicated the particulate composition detected by mass spectrometry (MS).

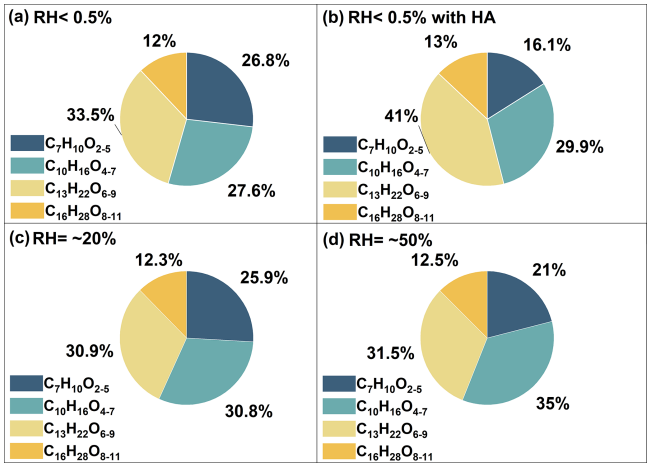

Figure 6. The proportion of compounds in sequence 2N generated during the myrcene ozonolysis under different conditions.

4 Conclusions

This study employed the MI-FTIR method to determine the presence of C3-CIs and C7-CIs during the myrcene ozonolysis. The O-O stretching vibration peak of C3-CIs was located at 880 cm^{-1}. The absence of characteristic infrared peaks belonged to C7-CIs, likely due to their low steady-state yield or rapid unimolecular decay. The characteristic IR peaks of acetone indirectly confirmed the production of C7-CIs.

Furthermore, combined with smog chamber experiments, it was verified that these two distinct CIs of different molecular sizes differ in their primary contribution mechanisms during SOA formation. For C3-CIs, they primarily underwent oligomerization reactions (e.g., $RO_2 + n$ C3-CIs + RO_2/HO_2) to form lower-volatility oligomers that incorporate into the particle. Meanwhile, the SCIs oligomerization and RO_2 autoxidation synergistically occurred during the myrcene ozonolysis, leading to the formation of HOMs-RO2 with higher oxygen content. To our knowledge, this was the first time this synergistic effect had been proposed. Larger C7-CIs primarily underwent unimolecular decomposition, producing C7-ROH and C7-RO_2. C7-ROH could be detected as a stable product in particle. The C7-RO_2 subsequently oligomerized with n C3-CIs to partition into the particle phase. The coexistence of carbon atoms with varying molecular sizes leads to a different role of CIs in SOA. SOA formation during the ozonolysis of myrcene, compared to that observed in cyclic monoterpenes (e.g., α-pinene and

limonene). The structural similarity of ocimene to myrcene meant its ozonolysis might also lead to CIs of varying sizes, potentially allowing for this synergistic effect. An increase in RH caused some SCIs to react directly with water, thereby reducing the fraction of SCIs that form oligomers and partition into the particle. This mechanism also significantly contributed to the decrease in SOA yield and the shift toward a smaller particle size distribution. Our study further deepened the understanding of monoterpene ozonolysis mechanisms, particularly from the perspective of Criegee chemistry.

Data availability. All raw data can be provided by the corresponding authors upon request.

Supplement. The supplement related to this article is available online at https://doi.org/10.5194/acp-26-2103-2026-supplement.

Author contributions. MFC and SRT planned the campaign; MFC, XFL and YYX performed the measurements; MFC and SSY analyzed the data; MFC wrote the manuscript draft; MFC, SRT, SST, HLZ and MFG reviewed and edited the manuscript.

Competing interests. The contact author has declared that none of the authors has any competing interests.

Disclaimer. Publisher's note: Copernicus Publications remains neutral with regard to jurisdictional claims made in the text, published maps, institutional affiliations, or any other geographical representation in this paper. The authors bear the ultimate responsibility for providing appropriate place names. Views expressed in the text are those of the authors and do not necessarily reflect the views of the publisher.

Acknowledgements. This work was supported by the National Key Research and Development Program of China (no. 2022YFC3700200), National Natural Science Foundation of China (contract nos. 42130606, 42430606), Beijing National Laboratory for Molecular Sciences (BNLMS-CXXM-202011).

Financial support. This research has been supported by the National Key Research and Development Program of China (grant no. 2022YFC3700200) and the National Natural Science Foundation of China (grant nos. 42130606 and 22321004).

Review statement. This paper was edited by Chiara Giorio and reviewed by Matti Rissanen and three anonymous referees.

References

Anglada, J. M. and Sole, A.: Impact of the water dimer on the atmospheric reactivity of carbonyl oxides, Phys. Chem. Chem. Phys., 18, 17698–17712, https://doi.org/10.1039/c6cp02531e, 2016.

Aschmann, S. M., Arey, J., and Atkinson, R.: OH radical formation from the gas-phase reactions of O_3 with a series of terpenes, Atmos. Environ., 36, 4347–4355, https://doi.org/10.1016/s1352-2310(02)00355-2, 2002.

Atkinson, R., Hasegawa, D., and Aschmann, S. M.: Rate constants for the gas-phase reactions of O_3 with a series of monoterpenes and related-compounds at 296 ± 2 K, Int. J. Chem. Kinet., 22, 871–887, https://doi.org/10.1002/kin.550220807, 1990.

Bach, S. B. H.: Matrix-Isolation Techniques: A Practical Approach. The Practical Approach in Chemistry Series By Ian R. Dunkin (University of Strathclyde), Oxford Press: New York, 1998, 242 pp., ISBN 0-19-855863-5, J. Am. Chem. Soc., 121, 5618–5618, https://doi.org/10.1021/ja9857099, 1999.

Baker, Y., Kang, S., Wang, H., Wu, R., Xu, J., Zanders, A., He, Q., Hohaus, T., Ziehm, T., Geretti, V., Bannan, T. J., O'Meara, S. P., Voliotis, A., Hallquist, M., McFiggans, G., Zorn, S. R., Wahner, A., and Mentel, T. F.: Impact of HO_2/RO_2 ratio on highly oxygenated α-pinene photooxidation products and secondary organic aerosol formation potential, Atmos. Chem. Phys., 24, 4789–4807, https://doi.org/10.5194/acp-24-4789-2024, 2024.

Boge, O., Mutzel, A., Iinuma, Y., Yli-Pirila, P., Kahnt, A., Joutsensaari, J., and Herrmann, H.: Gas-phase products and secondary organic aerosol formation from the ozonolysis and photooxidation of myrcene, Atmos. Environ., 79, 553–560, https://doi.org/10.1016/j.atmosenv.2013.07.034, 2013.

Boy, M., Mogensen, D., Smolander, S., Zhou, L., Nieminen, T., Paasonen, P., Plass-Dülmer, C., Sipilä, M., Petäjä, T., Mauldin, L., Berresheim, H., and Kulmala, M.: Oxidation of SO_2 by stabilized Criegee intermediate (sCI) radicals as a crucial source for atmospheric sulfuric acid concentrations, Atmos. Chem. Phys., 13, 3865–3879, https://doi.org/10.5194/acp-13-3865-2013, 2013.

Caravan, R. L., Bannan, T. J., Winiberg, F. A. F., Khan, M. A. H., Rousso, A. C., Jasper, A. W., Worrall, S. D., Bacak, A., Artaxo, P., Brito, J., Priestley, M., Allan, J. D., Coe, H., Ju, Y., Osborn, D. L., Hansen, N., Klippenstein, S. J., Shallcross, D. E., Taatjes, C. A., and Percival, C. J.: Observational evidence for Criegee intermediate oligomerization reactions relevant to aerosol formation in the troposphere, Nat. Geosci., 17, 219–226, https://doi.org/10.1038/s41561-023-01361-6, 2024.

Chao, W., Markus, C. R., Okumura, M., Winiberg, F. A. F., and Percival, C. J.: Chemical Kinetic Study of the Reaction of CH_2OO with CH_3O_2, J. Phys. Chem. Lett., 15, 3690–3697, https://doi.org/10.1021/acs.jpclett.4c00159, 2024.

Chen, L., Huang, Y., Xue, Y., Shen, Z., Cao, J., and Wang, W.: Mechanistic and kinetics investigations of oligomer formation from Criegee intermediate reactions with hydroxyalkyl hydroperoxides, Atmos. Chem. Phys., 19, 4075–4091, https://doi.org/10.5194/acp-19-4075-2019, 2019.

Chen, L., Huang, Y., Xue, Y., Jia, Z., and Wang, W.: Oligomer formation from the gas-phase reactions of Criegee intermediates with hydroperoxide esters: mechanism and kinetics, Atmos. Chem. Phys., 22, 14529–14546, https://doi.org/10.5194/acp-22-14529-2022, 2022.

Chen, M. F., Tong, S. R., Wang, Z., Li, W. R., Xu, Y. Y., Wang, S. F., and Ge, M. F.: Reaction mechanism and kinetics of Criegee intermediate and hydroperoxymethyl formate, J. Environ. Sci., 105, 128-137, https://doi.org/10.1016/j.jes.2020.12.029, 2021.

Chen, M. F., Tong, S. R., Yu, S. S., Xu, Y. Y., Lv, X. F., Zhang, H. L., Wang, S. F,, and Ge, M. F.: Impact of the Criegee Intermediate on the Formation of Secondary Organic Aerosols during E-4-Hexen-1-ol Ozonolysis, J. Phys. Chem. A, 129, 1704–1713, https://doi.org/10.1021/acs.jpca.4c08028, 2025.

Chen, T., Zhang, P., Chu, B., Ma, Q., Ge, Y., Liu, J., and He, H.: Secondary organic aerosol formation from mixed volatile organic compounds: Effect of RO_2 chemistry and precursor concentration, Npj Clim. Atmos. Sci., 5, 95, https://doi.org/10.1038/s41612-022-00321-y, 2022.

Chhantyal-Pun, R., Davey, A., Shallcross, D. E., Percival, C. J., and Orr-Ewing, A. J.: A kinetic study of the CH_2OO Criegee intermediate self-reaction, reaction with SO_2 and unimolecular reaction using cavity ring-down spectroscopy, Phys. Chem. Chem. Phys., 17, 3617–3626, https://doi.org/10.1039/c4cp04198d, 2015.

Chhantyal-Pun, R., Khan, M. A. H., Zachhuber, N., Percival, C. J., Shallcross, D. E., and Orr-Ewing, A. J.: Impact of Criegee Intermediate Reactions with Peroxy Radicals on Tropospheric Organic Aerosol, Acs Earth Space Chem., 4, 1743–1755, https://doi.org/10.1021/acsearthspacechem.0c00147, 2020.

Cox, R. A., Ammann, M., Crowley, J. N., Herrmann, H., Jenkin, M. E., McNeill, V. F., Mellouki, A., Troe, J., and Wallington, T. J.: Evaluated kinetic and photochemical data for atmospheric chemistry: Volume VII – Criegee intermediates, Atmos. Chem. Phys., 20, 13497–13519, https://doi.org/10.5194/acp-20-13497-2020, 2020.

Criegee, R.: Mechanism of Ozonolysis, Angew. Chem. Int. Edit., 14, 745–752, https://doi.org/10.1002/anie.197507451, 1975.

Deng, P., Wang, L., and Wang, L.: Mechanism of Gas-Phase Ozonolysis of β-Myrcene in the Atmosphere, J. Phys. Chem. A, 122, 3013–3020, https://doi.org/10.1021/acs.jpca.8b00983, 2018.

Donahue, N. M., Epstein, S. A., Pandis, S. N., and Robinson, A. L.: A two-dimensional volatility basis set: 1. organic-aerosol mixing thermodynamics, Atmos. Chem. Phys., 11, 3303–3318, https://doi.org/10.5194/acp-11-3303-2011, 2011.

Donahue, N. M., Kroll, J. H., Pandis, S. N., and Robinson, A. L.: A two-dimensional volatility basis set – Part 2: Diagnostics of organic-aerosol evolution, Atmos. Chem. Phys., 12, 615–634, https://doi.org/10.5194/acp-12-615-2012, 2012.

Frandsen, B. N., Franzon, L., Meder, M., Pasik, D., Ahongshangbam, E., Vinkvist, N., Myllys, N., Iyer, S., Rissanen, M. P., Ehn, M., and Kurtén, T. C.: Detailed Investigation of 2,3-Dimethyl-2-butene Ozonolysis-Derived Hydroxyl, Peroxy, and Alkoxy Radical Chemistry, ACS Earth Space Chem., 9, 1322–1337, https://doi.org/10.1021/acsearthspacechem.4c00355, 2025.

Frisch, M. J., Trucks, G. W., Schlegel, H. B., Scuseria, G. E., Robb, M. A., Cheeseman, J. R., Scalmani, G., Barone, V., Petersson, G. A., Nakatsuji, H., Li, X., Caricato, M., Marenich, A. V., Bloino, J., Janesko, B. G., Gomperts, R., Mennucci, B., Hratchian, H. P., Ortiz, J. V., Izmaylov, A. F., Sonnenberg, J. L., Williams, Ding, F., Lipparini, F., Egidi, F., Goings, J., Peng, B., Petrone, A., Henderson, T., Ranasinghe, D., Zakrzewski, V. G., Gao, J., Rega, N., Zheng, G., Liang, W., Hada, M., Ehara, M., Toyota, K., Fukuda, R., Hasegawa, J., Ishida, M., Nakajima, T., Honda, Y., Kitao, O., Nakai, H., Vreven, T., Throssell, K., Montgomery Jr., J. A., Peralta, J. E., Ogliaro, F., Bearpark, M. J., Heyd, J. J., Brothers, E. N., Kudin, K. N., Staroverov, V. N., Keith, T. A., Kobayashi, R., Normand, J., Raghavachari, K., Rendell, A. P., Burant, J. C., Iyengar, S. S., Tomasi, J., Cossi, M., Millam, J. M., Klene, M., Adamo, C., Cammi, R., Ochterski, J. W., Martin, R. L., Morokuma, K., Farkas, O., Foresman, J. B., and Fox, D. J.: Gaussian 16 Rev. A.03, Gaussian 16 Rev. A.03, Gaussian, Inc., Wallingford, CT, https://www.gaussian.com (last access: 8 February 2026), 2016.

Gong, Y. and Chen, Z.: Quantification of the role of stabilized Criegee intermediates in the formation of aerosols in limonene ozonolysis, Atmos. Chem. Phys., 21, 813–829, https://doi.org/10.5194/acp-21-813-2021, 2021.

Han, S. W. and Kim, K.: Infrared matrix isolation study of acetone and methanol in solid argon, J. Phys. Chem., 100, 17124–17132, https://doi.org/10.1021/jp961538n, 1996.

Harvey, R. M., Bateman, A. P., Jain, S., Li, Y. J., Martin, S., and Petrucci, G. A.: Optical Properties of Secondary Organic Aerosol from cis-3-Hexenol and cis-3-Hexenyl Acetate: Effect of Chemical Composition, Humidity, and Phase, Environ. Sci. Technol., 50, 4997–5006, https://doi.org/10.1021/acs.est.6b00625, 2016.

Hassan, Z., Stahlberger, M., Rosenbaum, N., and Braese, S.: Criegee Intermediates Beyond Ozonolysis: Synthetic and Mechanistic Insights, Angew. Chem. Int. Edit., 60, 15138–15152, https://doi.org/10.1002/anie.202014974, 2021.

Helmig, D., Daly, R. W., Milford, J., and Guenther, A.: Seasonal trends of biogenic terpene emissions, Chemosphere, 93, 35–46, https://doi.org/10.1016/j.chemosphere.2013.04.058, 2013.

Hofzumahaus, A., Rohrer, F., Lu, K. D., Bohn, B., Brauers, T., Chang, C. C., Fuchs, H., Holland, F., Kita, K., Kondo, Y., Li, X., Lou, S. R., Shao, M., Zeng, L. M., Wahner, A., and Zhang, Y. H.: Amplified Trace Gas Removal in the Troposphere, Science, 324, 1702–1704, https://doi.org/10.1126/science.1164566, 2009.

Jiang, H. T., Xie, C. L., Liu, Y., Xiao, C. L., Zhang, W. Q., Li, H. W., Long, B., Dong, W. R., Truhlar, D. G., and Yang, X. M.: Criegee Intermediates Significantly Reduce Atmospheric $(CF_3)_2CFCN$, J. Am. Chem. Soc., 147, 12263–12272, https://doi.org/10.1021/jacs.5c01737, 2025.

Jokinen, T., Sipila, M., Richters, S., Kerminen, V. M., Paasonen, P., Stratmann, F., Worsnop, D., Kulmala, M., Ehn, M., Herrmann, H., and Berndt, T.: Rapid Autoxidation Forms Highly Oxidized RO_2 Radicals in the Atmosphere, Angew. Chem. Int. Edit., 53, 14596–14600, https://doi.org/10.1002/anie.201408566, 2014.

Jr-Min Lin, J. and Chao, W.: Structure-dependent reactivity of Criegee intermediates studied with spectroscopic methods, Chem. Soc. Rev., 46, 7483–7497, https://doi.org/10.1039/C7CS00336F, 2017.

Khan, M. A. H., Percival, C. J., Caravan, R. L., Taatjes, C. A., and Shallcross, D. E.: Criegee intermediates and their impacts on the troposphere, Environ. Sci.-Proc. Imp., 20, 437–453, https://doi.org/10.1039/c7em00585g, 2018.

Kidwell, N. M., Li, H., Wang, X., Bowman, J. M., and Lester, M. I.: Unimolecular dissociation dynamics of vibrationally activated CH_3CHOO Criegee intermediates to OH radical products, Nature Chemistry, 8, 509–514, https://doi.org/10.1038/nchem.2488, 2016.

Kostiainen, R.: Volatile organic compounds in the indoor air of normal and sick houses, Atmos. Environ., 29, 693–702, https://doi.org/10.1016/1352-2310(94)00309-9, 1995.

Lelieveld, J., Gromov, S., Pozzer, A., and Taraborrelli, D.: Global tropospheric hydroxyl distribution, budget and reactivity, Atmos. Chem. Phys., 16, 12477–12493, https://doi.org/10.5194/acp-16-12477-2016, 2016.

Lin, H.-Y., Huang, Y.-H., Wang, X., Bowman, J. M., Nishimura, Y., Witek, H. A., and Lee, Y.-P.: Infrared identification of the Criegee intermediates syn- and anti-CH_3CHOO, and their distinct conformation-dependent reactivity, Nat. Commun., 6, 7012, https://doi.org/10.1038/ncomms8012, 2015.

Lin, L. C., Chang, H. T., Chang, C. H., Chao, W., Smith, M. C., Chang, C. H., Lin, J. J. M., and Takahashi, K.: Competition between H_2O and $(H_2O)(2)$ reactions with CH_2OO/CH_3CHOO, Phys. Chem. Chem. Phys., 18, 4557–4568, https://doi.org/10.1039/c5cp06446e, 2016.

Lin, Y.-H., Yin, C., Lin, W.-H., Li, Y.-L., Takahashi, K., and Lin, J. J.-M.: Criegee Intermediate Reaction with Alcohol Is Enhanced by a Single Water Molecule, J. Phys. Chem. Lett., 9, 7040–7044, https://doi.org/10.1021/acs.jpclett.8b03349, 2018.

Liu, D., Zhang, Y., Zhong, S., Chen, S., Xie, Q., Zhang, D., Zhang, Q., Hu, W., Deng, J., Wu, L., Ma, C., Tong, H., and Fu, P.: Large differences of highly oxygenated organic molecules (HOMs) and low-volatile species in secondary organic aerosols (SOAs) formed from ozonolysis of β-pinene and limonene, Atmos. Chem. Phys., 23, 8383–8402, https://doi.org/10.5194/acp-23-8383-2023, 2023.

Liu, S., Galeazzo, T., Valorso, R., Shiraiwa, M., Faiola, C. L., and Nizkorodov, S. A.: Secondary Organic Aerosol from OH-Initiated Oxidation of Mixtures of d-Limonene and beta-Myrcene, Environ. Sci. Technol., https://doi.org/10.1021/acs.est.4c04870, 2024.

Long, B., Bao, J. L., and Truhlar, D. G.: Unimolecular reaction of acetone oxide and its reaction with water in the atmosphere, Proc. Natl. Acad. Sci. USA, 115, 6135–6140, https://doi.org/10.1073/pnas.1804453115, 2018.

Long, B., Bao, J. L., and Truhlar, D. G.: Rapid unimolecular reaction of stabilized Criegee intermediates and implications for atmospheric chemistry, Nat. Commun., 10, 2003, https://doi.org/10.1038/s41467-019-09948-7, 2019.

Long, B., Xie, C., and Truhlar, D. G.: Criegee Intermediates Compete Well with OH as a Cleaning Agent for Atmospheric Amides, J. Am. Chem. Soc., https://doi.org/10.1021/jacs.5c07439, 2025.

Lu, T.: Molclus, Version 1.1.2., http://www.keinsci.com/research/molclus.html (last access: 6 November 2024), 2023.

Luo, Y., Franzon, L., Zhang, J., Sarnela, N., Donahue, N. M., Kurtén, T., and Ehn, M.: Gas-phase observations of accretion products from stabilized Criegee intermediates in terpene ozonolysis with two dicarboxylic acids, Atmos. Chem. Phys., 25, 4655–4664, https://doi.org/10.5194/acp-25-4655-2025, 2025.

Mauldin, R. L., Berndt, T., Sipilä, M., Paasonen, P., Petäjä, T., Kim, S., Kurtén, T., Stratmann, F., Kerminen, V. M., and Kulmala, M.: A new atmospherically relevant oxidant of sulphur dioxide, Nature, 488, 193-196, https://doi.org/10.1038/nature11278, 2012.

Munshi, H. B., Rao, K., and Iyer, R. M.: Rate constants of the reactions of ozone with nitriles, acrylates and terpenes in gas-phase, Atmos. Environ., 23, 1971–1976, https://doi.org/10.1016/0004-6981(89)90522-2, 1989.

Neese, F.: Software update: The ORCA program system-Version 5.0, WIREs Comput. Mol. Sci., https://doi.org/10.1002/wcms.1606, 2022.

Newland, M. J., Rickard, A. R., Sherwen, T., Evans, M. J., Vereecken, L., Muñoz, A., Ródenas, M., and Bloss, W. J.: The atmospheric impacts of monoterpene ozonolysis on global stabilised Criegee intermediate budgets and SO_2 oxidation: experiment, theory and modelling, Atmos. Chem. Phys., 18, 6095–6120, https://doi.org/10.5194/acp-18-6095-2018, 2018.

Peräkylä, O., Berndt, T., Franzon, L., Hasan, G., Meder, M., Valiev, R. R., Daub, C. D., Varelas, J. G., Geiger, F. M., Thomson, R. J., Rissanen, M., Kurtén, T., and Ehn, M.: Large Gas-Phase Source of Esters and Other Accretion Products in the Atmosphere, J. Am. Chem. Soc., 145, 7780–7790, https://doi.org/10.1021/jacs.2c10398, 2023.

Ringsdorf, A., Edtbauer, A., Vila-Guerau de Arellano, J., Pfannerstill, E. Y., Gromov, S., Kumar, V., Pozzer, A., Wolff, S., Tsokankunku, A., Soergel, M., Sa, M. O., Araujo, A., Ditas, F., Poehlker, C., Lelieveld, J., and Williams, J.: Inferring the diurnal variability of OH radical concentrations over the Amazon from BVOC measurements, Sci. Rep., 13, https://doi.org/10.1038/s41598-023-41748-4, 2023.

Sakamoto, Y., Inomata, S., and Hirokawa, J.: Oligomerization reaction of the Criegee intermediate leads to secondary organic aerosol formation in ethylene ozonolysis, J. Phys. Chem. A, 117, 12912–12921, https://doi.org/10.1021/jp408672m, 2013.

Sindelarova, K., Granier, C., Bouarar, I., Guenther, A., Tilmes, S., Stavrakou, T., Müller, J.-F., Kuhn, U., Stefani, P., and Knorr, W.: Global data set of biogenic VOC emissions calculated by the MEGAN model over the last 30 years, Atmos. Chem. Phys., 14, 9317–9341, https://doi.org/10.5194/acp-14-9317-2014, 2014.

Sipilä, M., Jokinen, T., Berndt, T., Richters, S., Makkonen, R., Donahue, N. M., Mauldin III, R. L., Kurtén, T., Paasonen, P., Sarnela, N., Ehn, M., Junninen, H., Rissanen, M. P., Thornton, J., Stratmann, F., Herrmann, H., Worsnop, D. R., Kulmala, M., Kerminen, V.-M., and Petäjä, T.: Reactivity of stabilized Criegee intermediates (sCIs) from isoprene and monoterpene ozonolysis toward SO_2 and organic acids, Atmos. Chem. Phys., 14, 12143–12153, https://doi.org/10.5194/acp-14-12143-2014, 2014.

Su, Y.-T., Huang, Y.-H., Witek, H. A., and Lee, Y.-P.: Infrared Absorption Spectrum of the Simplest Criegee Intermediate CH_2OO, Science, 340, 174–176, https://doi.org/10.1126/science.1234369, 2013.

Su, Y.-T., Lin, H.-Y., Putikam, R., Matsui, H., Lin, M. C., and Lee, Y.-P.: Extremely rapid self-reaction of the simplest Criegee intermediate CH_2OO and its implications in atmospheric chemistry, Nat. Chem., 6, 477–483, https://doi.org/10.1038/nchem.1890, 2014.

Taatjes, C. A., Welz, O., Eskola, A. J., Savee, J. D., Scheer, A. M., Shallcross, D. E., Rotavera, B., Lee, E. P. F., Dyke, J. M., Mok, D. K. W., Osborn, D. L., and Percival, C. J.: Direct Measurements of Conformer-Dependent Reactivity of the Criegee Intermediate CH_3CHOO, Science, 340, 177–180, https://doi.org/10.1126/science.1234689, 2013.

Vereecken, L., Harder, H., and Novelli, A.: The reaction of Criegee intermediates with NO, RO_2, and SO_2, and their fate in the atmosphere, Phys. Chem. Chem. Phys., 14, 14682–14695, https://doi.org/10.1039/c2cp42300f, 2012.

Vereecken, L., Novelli, A., and Taraborrelli, D.: Unimolecular decay strongly limits the atmospheric impact of Criegee intermediates, Phys. Chem. Chem. Phys., 19, 31599–31612, https://doi.org/10.1039/c7cp05541b, 2017.

Vereecken, L., Novelli, A., Kiendler-Scharr, A., and Wahner, A.: Unimolecular and water reactions of oxygenated and unsaturated Criegee intermediates under atmospheric conditions, Phys. Chem. Chem. Phys., 24, 6428-6443, https://doi.org/10.1039/d1cp05877k, 2022.

Wang, Y.-Y., Chung, C.-Y., and Lee, Y.-P.: Infrared spectral identification of the Criegee intermediate $(CH_3)_2COO$, J. Chem. Phys., 145, 154303, https://doi.org/10.1063/1.4964658, 2016.

Wang, Z., Tong, S. R., Chen M. F., Jing, B., Li, W. R., Guo, Y. C., Ge, M. F., and Wang, S. F.: Study on ozonolysis of asymmetric alkenes with matrix isolation and FT-IR spectroscopy, Chemosphere, 252, 126413, https://doi.org/10.1016/j.chemosphere.2020.126413, 2020.

Welz, O., Eskola, A. J., Sheps, L., Rotavera, B., Savee, J. D., Scheer, A. M., Osborn, D. L., Lowe, D., Booth, A. M., Xiao, P., Khan, M. A. H., Percival, C. J., and Shallcross, D. E.: Rate Coefficients of C1 and C2 Criegee Intermediate Reactions with Formic and Acetic Acid Near the Collision Limit: Direct Kinetics Measurements and Atmospheric Implications, Angew. Chem. Int. Edit., 53, 4547–4550, https://doi.org/10.1002/anie.201400964, 2014.

Yang, X., Deng, J., Li, D., Chen, J., Xu, Y., Zhang, K., Shang, X., and Cao, Q.: Transient species in the ozonolysis of tetramethylethene, J. Environ. Sci., 95, 210–216, https://doi.org/10.1016/j.jes.2020.03.027, 2020.

Yin, C. and Takahashi, K.: Effect of unsaturated substituents in the reaction of Criegee intermediates with water vapor, Phys. Chem. Chem. Phys., 20, 20217–20227, https://doi.org/10.1039/c8cp02064g, 2018.

Yu, S. S., Tong, S. R., Chen, M. F., Zhang, H. L., Xu, Y. Y., Guo, Y. C., and Ge, M. F.: Characterization of Key Intermediates and Products from the Ozonolysis of Styrene-Like Compounds, Environ. Sci. Technol., https://doi.org/10.1021/acs.est.5c00769, 2025.

Zhang, D. and Zhang, R.: Ozonolysis of alpha-pinene and beta-pinene: Kinetics and mechanism, J. Chem. Phys., 122, https://doi.org/10.1063/1.1862616, 2005.

Zhang, S., Du, L., Yang, Z., Tchinda, N. T., Li, J., and Li, K.: Contrasting impacts of humidity on the ozonolysis of monoterpenes: insights into the multi-generation chemical mechanism, Atmos. Chem. Phys., 23, 10809–10822, https://doi.org/10.5194/acp-23-10809-2023, 2023.

Zhao, Q., Wang, W., Liu, F., Lu, J., and Wang, W.: Oligomerization reactions for precursors to secondary organic aerosol: Comparison between two formation mechanisms for the oligomeric hydroxyalkyl hydroperoxides, Atmos. Environ., 166, 1–8, https://doi.org/10.1016/j.atmosenv.2017.07.008, 2017.

Zhao, Y., Wingen, L. M., Perraud, V., Greaves, J., and Finlayson-Pitts, B. J.: Role of the reaction of stabilized Criegee intermediates with peroxy radicals in particle formation and growth in air, Phys. Chem. Chem. Phys., 17, 12500–12514, https://doi.org/10.1039/c5cp01171j, 2015.

Zhao, Z., Zhang, W., Alexander, T., Zhang, X., Martin, D. B. C., and Zhang, H.: Isolating α-Pinene Ozonolysis Pathways Reveals New Insights into Peroxy Radical Chemistry and Secondary Organic Aerosol Formation, Environ. Sci. Technol., 55, 6700–6709, https://doi.org/10.1021/acs.est.1c02107, 2021.